THE JOURNAL OF BIOLOGICAL CHEMISTRY VOL. 285, NO. 9, pp. 6725–6738, February 26, 2010
© 2010 by The American Society for Biochemistry and Molecular Biology, Inc. Printed in the U.S.A.

ERp57 Modulates STAT3 Signaling from the Lumen of the Endoplasmic Reticulum*[S]

Received for publication, August 8, 2009, and in revised form, December 7, 2009 Published, JBC Papers in Press, December 18, 2009, DOI 10.1074/jbc.M109.054015

Helen Coe[‡§1], **Joanna Jung**[‡1], **Jody Groenendyk**[‡2], **Daniel Prins**[‡3], **and Marek Michalak**[‡§4]

From the Departments of [‡]*Biochemistry and* [§]*Pediatrics, School of Molecular and Systems Medicine, University of Alberta, Edmonton, Alberta T6G 2H7, Canada*

ERp57 is an endoplasmic reticulum (ER) resident thiol disulfide oxidoreductase. Using the gene trap technique, we created a ERp57-deficient mouse model. Targeted deletion of the *Pdia3* gene, which encodes ERp57, in mice is embryonic lethal at embryonic day (E) 13.5. β-Galactosidase reporter gene analysis revealed that ERp57 is expressed early on during blastocyst formation with the highest expression in the inner cell mass. In early stages of mouse embryonic development (E11.5) there is a relatively low level of expression of ERp57. As the embryos developed, ERp57 became highly expressed in both the brain and the lungs (E15.5 and E18.5). The absence of ERp57 has no impact on ER morphology; expression of ER-associated chaperones and folding enzymes, ER stress, or apoptosis. ERp57 has been reported to interact with STAT3 (signal transducer and activator of transcription)-DNA complexes. We show here that STAT3-dependent signaling is increased in the absence of ERp57 and this can be rescued by expression of ER-targeted ERp57 but not by cytoplasmic-targeted protein, indicating that ERp57 affects STAT3 signaling from the lumen of the ER. ERp57 effects on STAT3 signaling are enhanced by ER luminal complex formation between ERp57 and calreticulin. In conclusion, we show that ERp57 deficiency in mouse is embryonic lethal at E13.5 and ERp57-dependent modulation of STAT3 signaling may contribute to this phenotype.

The endoplasmic reticulum (ER)[5] is involved in many cellular functions including protein synthesis and modification, regulation of Ca^{2+} homeostasis, phospholipid and steroid synthesis, and regulation of the response to cellular stress (1–3). To carry out these diverse functions, the ER is equipped with many chaperone proteins and folding enzymes (3). For example, calreticulin, calnexin, and the oxidoreductase ERp57 are components of the folding machinery involved in quality control of newly synthesized glycoproteins (3). ERp57 forms complexes with calnexin and calreticulin to assist in chaperone functions to ensure that newly synthesized proteins are correctly folded (3). Targeted deletion of ERp57 in B cells in mice results in normal B cell development and proliferation as well as antibody production (4). However, there is aberrant assembly of the peptide loading complex indicating that ERp57 is involved in the assembly of the peptide loading complex and this protein contributes both qualitatively and quantitatively to major histocompatibility complex (MHC) class I antigen presentation *in vivo* (4). Interestingly, small interfering RNA studies also demonstrate that ERp57 might be critical for oxidative folding of immunoglobulin heavy chain but not important for peptide loading of class I molecules (5).

Aside from its role as a folding enzyme in quality control in the secretory pathway, ERp57, also known as glucose-regulated protein 58 or Grp58 (6–13) has been reported to affect STAT3 (signal transducers and activators of transcription) signaling via interaction with STAT3 (6, 14–17). STATs are a family of cytoplasmic proteins with Src homology 2 domains that act as signal messengers and transcription factors as a part of the Janus kinase-STAT pathway (18). Upon activation, STAT proteins become phosphorylated on a specific tyrosine residue by activated Janus kinases and subsequently dimerize and translocate to the nucleus where they bind to specific DNA sequences to regulate the expression of target genes (18, 19). Among the STAT proteins, STAT3 has been implicated in transduction of the cellular signals that are involved in the regulation of cardiac growth, development, and hypertrophy (20). Although it is not clear how STAT3 activity is negatively regulated by ER resident ERp57, it has been reported that ERp57 may sequester the inactive and active STAT3 preventing its interaction with DNA and consequently activation of STAT3-dependent genes (6, 12).

In this study we created ERp57-deficient mice and *ERp57*$^{-/-}$ cell lines. ERp57 deficiency was embryonic lethal at embryonic day 13.5 (E13.5) and ERp57-deficient cells had significantly increased STAT3 activity. We showed that the ER, but not cytoplasmic, form of ERp57 is responsible for inhibition of STAT3 activity. Furthermore, ERp57-dependent modulation of STAT3 was enhanced by ER luminal interactions between

* This work was supported in part by Canadian Institutes of Health Research Grant MOP-15291, the Heart and Stroke Foundation of Alberta, and the Alberta Heritage Foundation for Medical Research.

[S] The on-line version of this article (available at http://www.jbc.org) contains supplemental Fig. S1.

[1] Recipients of studentship awards from the Alberta Heritage Foundation for Medical Research.

[2] Supported by the Canadian Institutes of Health Research, Heart and Stroke Foundation of Canada Membrane Protein and the Cardiovascular Disease Training Program.

[3] Supported by an Alberta Heritage Foundation for Medical Research Summer Studentship and the Canadian Institutes of Health Research Frederick Banting and Charles Best Canada Graduate Scholarship Master's Award.

[4] To whom correspondence should be addressed. Tel.: 780-492-2256; Fax: 780-492-0886; E-mail: marek.michalak@ualberta.ca.

[5] The abbreviations used are: ER, endoplasmic reticulum; BFA, brefeldin A; E, embryonic day; *ERp57*$^{-/-}$-ERp57$_{ER}$, ERp57-deficient cells expressing ER targeted ERp57; *ERp57*$^{-/-}$-ERp57$_{cyt}$, ERp57-deficient cells expressing cytoplasmic targeted ERp57; FACS, fluorescence-activated cell sorting; GAPDH, glyceraldehyde-3-phosphate dehydrogenase; MHC, major histocompatibility complex; PBS, phosphate-buffered saline; PDI, protein-disulfide isomerase; RT, reverse transcription; STAT, signal transducers and activators of transcription; UPR, unfolded protein responses; Xbp, X-box-binding protein; GFP, green fluorescent protein.

ERp57 and calreticulin. Our results suggest that, *in vivo*, ERp57 and STAT3 may not interact and that the observed modulation of STAT3 activity may be due to ERp57-dependent signaling from the ER.

EXPERIMENTAL PROCEDURES

Generation of ERp57-deficient Mice—Gene trapping with the trap vector pGT1TMpfs was used to generate the *Pdia3* gene disrupted embryonic stem cells from the Gene Trap Resource (BayGenomics, University of San Francisco, San Francisco, CA). The *Pdia3* gene encodes ERp57. Parental cell lines (CGR8 and E14Tg2A) were established from delayed blastocysts on gelatinized tissue culture dishes in embryonic stem cell medium containing leukemia inhibitory factor (21). Embryonic stem cells were cultured in medium containing Glasgow minimal essential medium, 2 mM glutamine, 1 mM sodium pyruvate, non-essential amino acids, 10% fetal calf serum, 100 nM β-mercaptoethanol, and 1000 units of leukemia inhibitory factor (22). Embryonic stem cells were microinjected into 3.5-day-old C57BL/6J blastocysts to generate chimeric mice (23). Chimeric males were analyzed for germline transmission by mating with C57BL/6J females, and the progeny were identified by PCR analysis, β-galactosidase staining, and Western blot analysis. All animal experimental procedures were approved by the Animal Welfare Program at the Research Ethics Office, University of Alberta, and conformed to relevant regulatory standards.

Genotype Analysis of ERp57-deficient Mice—Genomic DNA from heterozygous mice (carrying the *LacZ* gene) was isolated using the DNeasy Blood and Tissue kit (Invitrogen). Genomic DNA was purified using a PCR purification kit (Qiagen), and then DNA fragments were ligated using the Rapid DNA Ligation Kit (Boehringer). First, PCR amplification was performed using primers specific to the inserted vectors: INVF1, 5′-GTTCCCAACGATCAAGGCGAG-3′; and INVR1, 5′-AAGCCATACCAAACGACGAGCG-3′. The product from the PCR was used as a template for a second PCR with specific (nested) primers: INVF2, 5′-TCAAGGCGAGTTACATGATCCC-3′, and INVR2, 5′-CGAGCGTGACACCACGATGC-3′. Products of the inverse PCR-driven amplification were analyzed by agarose gel electrophoresis, purified using a gel purification kit (Qiagen), and sequenced. Once the integration site was identified, a protocol was designed for genotyping wild-type, heterozygote, and homozygote ERp57-deficient embryos (Fig. 1). Embryos were harvested at embryonic days 10.5–15.5 followed by isolation of genomic DNA. The following PCR primers were used for genotyping wild-type embryos: forward primer (F2), 5′-GGACAGTTTTGAGCTGCCAT-3′ (hybridizes to the intron within the insertion of the vector site) and reverse primer (R3), 5′-TCTCCATTATCATCGTACTCC-3′ (hybridizes to intron 4 after the vector insertion site). To identify heterozygous embryos the following primers were used: forward primer (F1), 5′-TCAAGGCGAGTTACATGATCCC-3′ (hybridizes to the end of the inserted vector) and reverse primer R3.

Histological Analysis—Blastocysts were harvested at 3 days post-coitum and whole mount β-galactosidase staining of blastocysts was performed. Blastocysts were washed with phosphate-buffered saline (PBS), fixed in 3.7% paraformaldehyde in PBS for 30 min, then washed with PBS. Blastocysts were then incubated for 1 h in freshly prepared staining solution in 10 ml of PBS containing 2 mM $MgCl_2$, 0.01% sodium deoxycholate, 0.02% Nonidet P-40, and 0.1% 5-bromo-4-chloro-3-indoyl-β-D-galactopyranoside (X-gal) dissolved in dimethyl formamide (24). Photographs of blastocysts were taken using a Nikon Coolpix 995 camera attached to a Nikon eclipse TS100 microscope with a ×10 magnification objective. β-Galactosidase, hematoxylin, and eosin staining of wild-type and $ERp57^{+/-}$ embryos was carried out as described previously (2). β-Galactosidase-stained slides were counterstained with eosin (0.1% eosin in 0.1% acetic acid). Embryos were viewed with the Nikon CoolscanIV.

Cell Culture, Plasmid DNA, DNA Cloning, and Lentivirus Transduction—Mouse embryonic fibroblasts were isolated from day 11 wild-type and ERp57-deficient embryos, immortalized, and maintained in culture as described previously (23). When indicated, cells were treated with 1 μM thapsigargin or 2.5 μM brefeldin A for 16 h.

cDNAs encoding full-length ERp57 or encoding mature ERp57 with no signal sequence were isolated from a mouse brain cDNA library using Gateway Cloning Technology (Invitrogen). The following forward DNA primers were used for amplification of full-length ERp57 and no signal sequence: ERp57, 5′-GGGG**ACAAGTTTGTACAAAAAAGCAGGCT**-AT*ACCATG*CGCTTCAGCTGCCTAGCT-3′ and 5′-GGG-G**ACAAGTTTGTACAAAAAAGCAGGCT**AT*ACCATG*G-ATGTGTTGGAACTGACGGACGA-3′, respectively. The forward primers contain an *att*B1 recombination site (bold), Kozak sequence for expression in mammalian cells (italics), and gene-specific nucleotides (underlined). The same reverse primer was used for the synthesis of cDNAs encoding full-length and no signal sequence ERp57: 5′-GGGG**ACCACT-TTGTACAAGAAAGCTGGGT**CCTAGAGGTCTCTTGT-GCCTTCTT-3′. The reverse primer contained an *att*B2 recombination site (bold) and the ERp57 gene-specific nucleotides (underlined). Both forward and reverse primers required four guanine residues at the 5′ end. First, a BP clonase reaction was carried out as recommended by the manufacturer to generate entry clone vectors. A recombination reaction was carried out using BP Clonase Enzyme Mix to insert cDNA encoding full-length ERp57 or no signal sequence ERp57 with the promoter EF1α (cellular polypeptide chain elongation factor 1α) into the destination lentiviral vector $2K7_{bsd}$ (containing a blasticidine resistance gene for cell selection). Expression vectors $p2K7ERp57_{ER}$ and $p2K7ERp57_{cyt}$ contained cDNA encoding full-length ERp57 and no signal sequence ERp57, respectively. Lentiviral transduction techniques were used to generate $ERp57^{-/-}$ and wild-type fibroblast-derived cells lines stably expressing recombinant proteins ERp57 or no signal sequence ERp57 (25). Protein from the bulk cell population was harvested with RIPA buffer containing 50 mM Tris, pH 7.5, 150 mM NaCl, 1 mM EDTA, 1 mM EGTA, 1% Triton X-100, 0.1% SDS, 0.5% sodium deoxycholate, and protease inhibitors (0.5 mM phenylmethylsulfonyl fluoride, 0.5 mM benzamidine, 0.05 μg/ml of aproprotin, 0.025 μg/ml of phosphormidone, 0.05 μg/ml of N^{α}-*p*-tosyl-L-lysine chloromethylketone, 0.05 μg/ml of 4-amidinophenyl)-methanesulfonyl fluoride hydrochloride monohydrate, 0.05 μg/ml of (2*S*,3*S*)-3-(*N*-carbamoyl)oxirane-

2-carboxylic acid (E-64), 0.025 μg/ml of leupeptin, and 0.01 μg/ml of pepstatin) (26). Expression of full-length ER-targeted ERp57 and cytoplasmically targeted ERp57 (no signal sequence ERp57) was monitored by Western blot analysis (2, 25, 27). ERp57-deficient cells expressing full-length ERp57 were denoted *ERp57*$^{-/-}$-ERp57$_{ER}$ and cells expressing no signal sequence-cytoplasmic ERp57 were denoted *ERp57*$^{-/-}$-ERp57$_{cyt}$.

SDS-PAGE and Western Blot Analysis—Whole cell lysates from wild-type, *ERp57*$^{-/-}$, *ERp57*$^{-/-}$-ERp57$_{ER}$, and *ERp57*$^{-/-}$-ERp57$_{cyt}$ mouse embryonic fibroblasts were isolated as described previously (2). Twenty μg of protein was separated by SDS-PAGE (10% acrylamide), transferred to nitrocellulose, and probed with specific antibodies (28). Antibodies used were rabbit anti-Grp78/BiP at a dilution of 1:1000 (StressGen), rabbit anti-calnexin at a dilution of 1:1000 (StressGen), goat anti-calreticulin at a dilution of 1:300, rabbit anti-ERp57 at a dilution of 1:1000, rabbit anti-protein-disulfide isomerase (PDI) at a dilution of 1:1000, rabbit anti-ERp41 at a dilution of 1:1000, rabbit anti-ERp54 at a dilution of 1:1000, and rabbit anti-β-tubulin (Abcam) at a dilution of 1:1000 (2, 29).

For detection of phosphorylated-STAT3 (Tyr^{705}-phospho-STAT3), *ERp57*$^{-/-}$, *ERp57*$^{-/-}$-ERp57$_{ER}$, and *ERp57*$^{-/-}$-ERp57$_{cyt}$ cells were grown to confluence and treated with 2 mM Na_3VO_4 for 20 min prior to harvesting. Cells were washed with PBS containing 4 mM Na_3VO_4 and harvested in RIPA buffer. Thirty μg of protein was separated by SDS-PAGE (10% acrylamide) and transferred to nitrocellulose membrane (28). The nitrocellulose membrane was washed with 25 ml of TBS buffer containing 20 mM Tris, pH 7.6, and 150 mM NaCl, and blocked for 1 h in TBS containing 5% milk and 0.1% Tween 20. Membranes were probed with rabbit anti-phospho-STAT3 (Tyr^{705}) antibodies (Cell Signaling) or anti-STAT3 (Cell Signaling) at 1:1,000 dilutions overnight at 4 °C. Secondary antibodies used were goat anti-rabbit (1:10,000 or 1:15,000 for anti-phospho-STAT3 antibodies) (Cell Signaling) and rabbit anti-goat (1:10,000 for anti-STAT3 antibodies) (Cell Signaling). Blots were developed using a chemiluminescent system (28).

Reverse Transcription (RT)-PCR—Total RNA was isolated from different tissues using TRIzol Reagent (Invitrogen). cDNA was synthesized using Moloney murine leukemia virus reverse transcriptase (Invitrogen) and amplified with *Taq* polymerase (Sigma) using the following primers: for ERp57, forward primer 5′-GGACAGTTTTGAGCTGCCAT-3′ and reverse primer 5′-CTCTCCATTATCATCGTACTCC-3′; for Xbp1, forward primer 5′-CCTTGTGGTTGAGAACCAGG-3′ and reverse primer 5′-CTAGAGGCTTGGTGTATAC-3′; for Grp78, forward primer 5′-TGGTATTCTCCGAGTGACAGC-3′ and reverse primer 5′-AGTCTTCAATGTCCGCATCC-3′; for glyceraldehyde-3-phosphate dehydrogenase (GAPDH), forward 5′-AACTTTGGCATTGTGGAAGG-3′ and reverse primer 5′-ACACATTGGGGGTAGGAACA-3′; and for STAT3, 5′-AGTCACATGCCACGTTGGTGTTTC-3′ and reverse primer 5′-CGGGCAATTTCCATTGGCTTCTCA-3′.

Immunohistochemistry and Electron Microscopy—For immunostaining, *ERp57*$^{-/-}$, *ERp57*$^{-/-}$-ERp57$_{ER}$, and *ERp57*$^{-/-}$-ERp57$_{cyt}$ mouse embryonic fibroblasts were grown on glass coverslips. Cells were fixed with 3.7% paraformaldehyde in PBS for 20 min at room temperature (2). For immunostaining of ERp57, cells were permeabilized with 0.1% Triton X-100 in PBS for 20 min at room temperature and washed twice with PBS. Cells were incubated in PBS containing 1% bovine serum albumin for 30 min at room temperature and then incubated with anti-ERp57 (1:100) in PBS containing 1% bovine serum albumin for 1 h at room temperature. The secondary antibody used was rabbit-conjugated fluorescein isothiocyanate (Invitrogen) at a dilution of 1:100 in PBS containing 1% bovine serum albumin for 45 min at room temperature (30). All coverslips were co-stained with Alexa Fluor 546-concanavalin A at a dilution of 1:1000 (Sigma). The coverslips were mounted onto glass slides and fluorescent signals visualized using spinning disk confocal microscopy (WaveFX from Quorum Technologies, Guelph, Canada) set up on an Olympus IX-81 inverted stand (Olympus, Markham, Canada). Images were acquired through a ×60 objective (N.A. 1.42) with an EMCCD camera (Hamamatsu, Japan). The fluorescent dyes, fluorescein isothiocyanate and Texas Red, were excited by 491- and 561-nm laser lines, respectively (Spectral Applied Research, Richmond Hill, Canada). Z-slices (0.25 μm) were acquired using Volocity (Improvision) through the cells using a piezo z-stage (Applied Scientific Instrumentation, Eugene, OR).

For electron microscopy analysis, cells were harvested, spun down, and fixed at 4 °C for 4 h in a freshly prepared solution containing 2.5% glutaraldehyde and 2% paraformaldehyde in 100 mM cacodylate, pH 7.2 (31). Samples were processed for electron microscopy and examined with a Hitachi Transmission Electron Microscope H-7000.

Subcellular Fractionation—Wild-type, *ERp57*$^{-/-}$, and *ERp57*$^{-/-}$-ERp57$_{cyt}$ cells harvested in a buffer containing of 250 mM sucrose, 20 mM Hepes, pH 7.0, 10 mM KCl, 1.5 mM $MgCl_2$, 1 mM EDTA, 1 mM EGTA, 1 mM dithiothreitol, 200 μM phenylmethylsulfonyl fluoride, 100 μM benzamidine, and protease inhibitors (26). The cellular suspension was incubated on ice for 10 min, then subjected to 40 strokes with a Dounce homogenizer followed by a 20-min incubation on ice. The sample was centrifuged at 720 × *g* for 5 min, and the supernatant containing cytoplasm, mitochondria, and membranes was centrifuged at 10,000 × *g* for 10 min. The supernatant containing cytoplasm and membranes was then subjected to a high speed centrifuge at 100,000 × *g* for 1 h to separate the cytoplasmic fraction from the pellet containing the ER-enriched membrane vesicles. Membrane pellet was suspended in 1 ml of RIPA buffer containing 50 mM Tris, pH 7.2, 150 mM NaCl, 1 mM EDTA, 1 mM EGTA, 1% Triton X-100, 0.1% SDS, 0.5% sodium deoxycholate, 200 μM phenylmethylsulfonyl fluoride, 100 μM benzamidine, and protease inhibitors (26). Prior to SDS-PAGE proteins were precipitated with ice-cold acetone. Proteins were transferred to nitrocellulose membrane followed by Western blot analysis with rabbit anti-ERp57 antibodies at a dilution of 1:1,000.

FACS Analysis—Samples were analyzed on BD FACScan single laser flow cytometry (BD Bioscience) equipped with a 488-nm filter. Data were collected from 10,000 cells and analyzed using CellQuest software. Cells at confluence of 80–90% were harvested by scraping into PBS, re-suspended in 100 μl of 0.1% formaldehyde in PBS, and incubated for 30 min with rab-

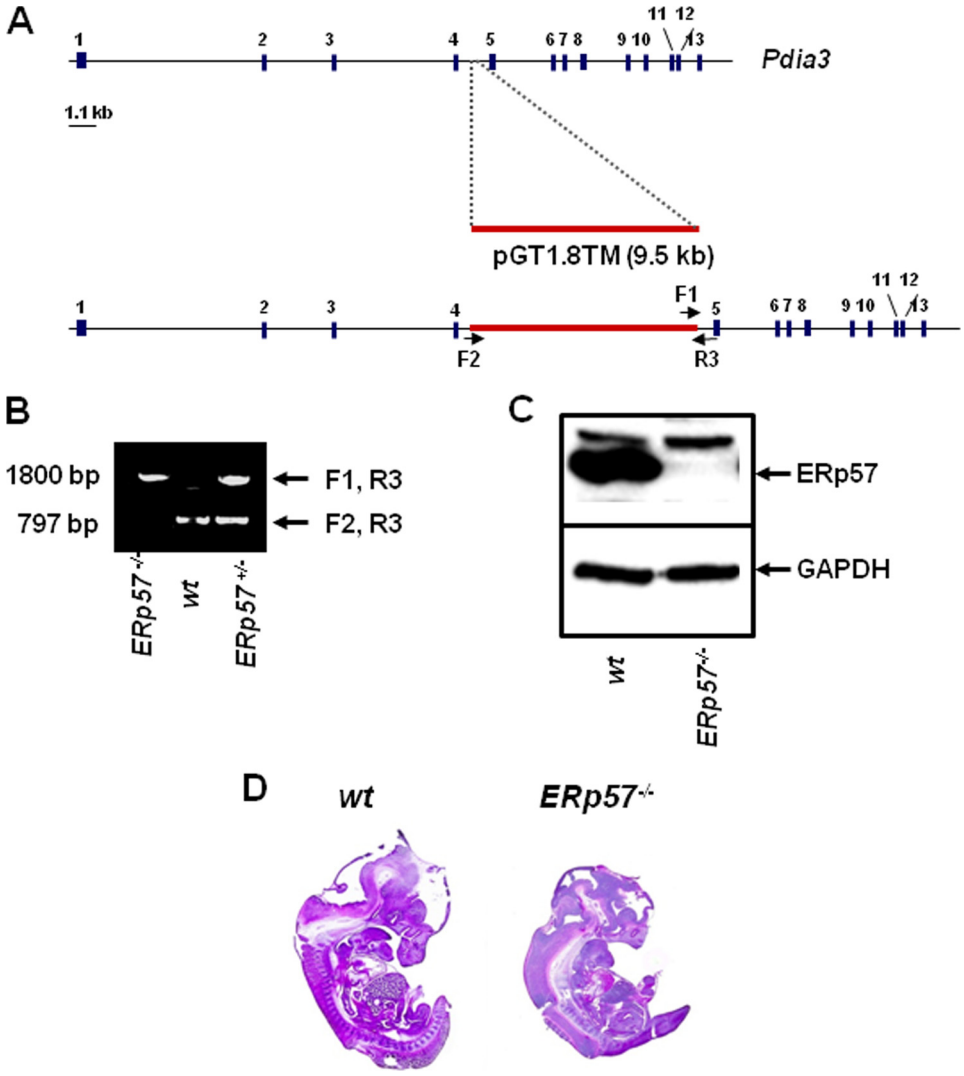

FIGURE 1. **Disruption of the ERp57 gene and generation of *ERp57*$^{-/-}$ *mice.*** *A*, a linear representation of the *Pdia3* gene that encodes ERp57. The gene was interrupted by insertion of the pGT1.8TM vector (*red*). The locations of the F1, F2, and R3 DNA primers used for genotyping are indicated in the figure. Introns are represented as *blocks*. *B*, PCR analysis of genomic DNA isolated from wild-type (*wt*), heterozygote *ERp57*$^{+/-}$, and homozygote *ERp57*$^{-/-}$ embryos. Primers R3 and F1 were used for detection of wild-type alleles and R3 and F2 for mutated alleles. *C*, Western blot analysis with anti-ERp57 antibodies (*upper panel*). The *lower* protein band corresponds to a nonspecific immunoreactivity. Anti-glyceraldehyde-3-phosphate dehydrogenase (*GAPDH*) antibodies were used to normalize for protein loading (*lower panel*). *D*, hematoxylin and eosin staining of embryonic day 12.5 wild-type (*wt*) and ERp57-deficient embryos (*ERp57*$^{-/-}$).

TABLE 1
Genotyping of offspring from ERp57$^{+/-}$ intercross

Age of mouse	Number of progeny	ERp57 genotype		
		+/+	+/−	−/−
E15.5	6	1	5	0
E14.5	5	2	3	0
E13.5	11	3	7	1
E12.5	8	2	5	1
E11.5	15	8	4	3
E10.5	9	2	5	2
Total	54	18	24	7

bit anti-ERp57 antibodies at a concentration of 1:150. Pelleted cells were than washed 3 times with PBS containing 2% fetal bovine serum followed by addition of fluorescein isothiocyanate-labeled anti-rabbit (Alexa Fluor 488; Invitrogen) secondary antibody. Cells were washed 3 times with PBS with fetal bovine serum and once with PBS alone. Staining with secondary antibodies alone was used as a negative control. All experiments were carried out at least three times.

Luciferase Reporter Gene Assay—Generation of *crt*$^{-/-}$, *crt*$^{-/-}$-CRT^{G242A}, and *crt*$^{-/-}$-CRT^{E234R} mouse embryonic fibroblasts was described previously (32). *ERp57*$^{-/-}$ and *ERp57*$^{-/-}$-ERp57$_{ER}$ cells were transfected with ER stress luciferase reporter vector (pRL-XFL, a generous gift from Dr. R. J. Kaufman (33)) as described previously (2). Twenty four hours after transfection, cells were treated with thapsigargin (1 μM) or H_2O_2 (50 μM) for 16 h. *ERp57*$^{-/-}$, *ERp57*$^{-/-}$-ERp57$_{ER}$, *ERp57*$^{-/-}$-ERp57$_{cyt}$, *crt*$^{-/-}$, *crt*$^{-/-}$-CRT, *crt*$^{-/-}$-CRT^{G242A}, and *crt*$^{-/-}$-CRT^{E234R} cells were co-transfected with a luciferase reporter gene under control of the STAT3 promoter (pLucTKS3, a kind gift from Dr. J. Jung and was described previously (34, 35)) with a *Renilla* luciferase reporter ratio of 50:1, respectively (2). After 48 h cells were harvested, lysed, and collected in Passive Lysis Buffer (Promega) followed by measurement of luciferase activity using the Dual Luciferase Assay Kit (Promega) and a Berthold-Lumat 9507 luminometer (2). Relative light units were normalized to the *Renilla* luciferase under the control of the cytomegalovirus promoter (2, 33). Four independent transfection experiments were carried out. Statistics were performed using two-sample unpaired *t* tests.

Miscellaneous Procedures—Protein concentration was measured spectrophotometrically using a Bio-Rad procedure (2). Ca^{2+} fluorescence measurements were carried out using 0.5 μM Fura2-AM (22). Cells were treated with 600 nM bradykinin and 300 nM thapsigargin (36). Each trial was calibrated with 1 μM ionomycin and 4 mM $CaCl_2$ to obtain a maximum value and with 30 mM EGTA, 25 mM Tris-HCl, pH 7.4, and 0.4% Triton X-100 to obtain a minimum value. Fluorescence was measured at λ_{ex} = 340 nm, λ_{ex} = 380 nm, and λ_{em} = 510 nm. Ca^{2+} concentrations were calculated from the fluorescence values.

RESULTS

ERp57 Deficiency Is Embryonic Lethal—Fig. 1*A* summarizes the results of the gene trapping strategy used to generate ERp57-deficient mice. The *Pdia3* gene, which encodes

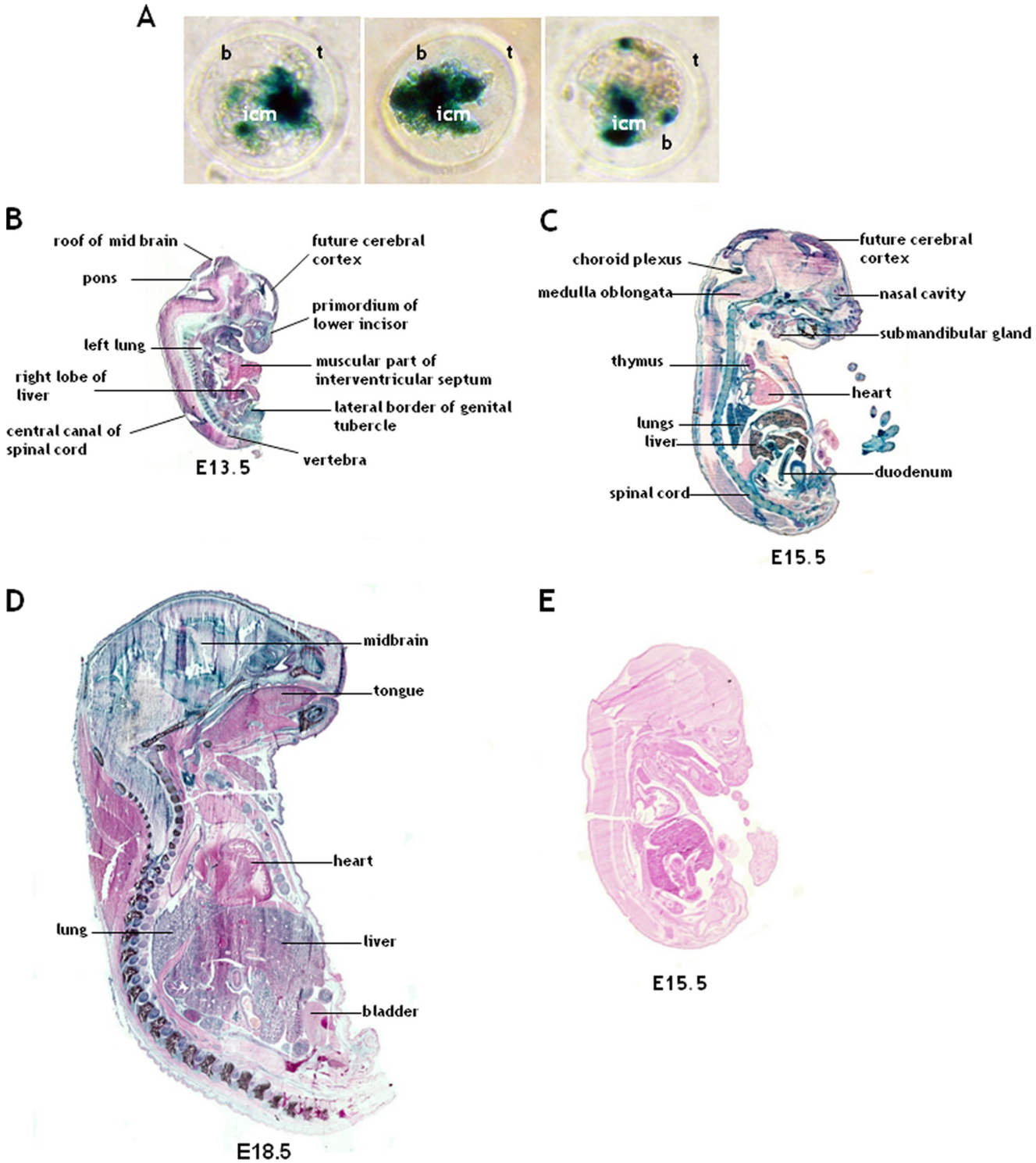

FIGURE 2. **Activation of the ERp57 promoter during mouse embryogenesis.** Expression of the ERp57 gene was detected as β-galactosidase activity from the β-galactosidase reporter gene inserted in the ERp57 gene within the *ERp57*$^{+/-}$ mouse (see Fig. 1). *A*, activation of the ERp57 promoter in mouse blastocysts. High activation of the ERp57 gene was detected in the inner cell mass (*icm*) of the blastocysts but not in the blastocoels (*b*) or trophoblasts (*t*). *B*, activation of the ERp57 promoter in lung, liver, and spine but not the heart of E13.5 *ERp57*$^{+/-}$ mouse embryos. *C*, high activity of the ERp57 promoter in the lung, liver, gut, and spinal cord in an E15.5 *ERp57*$^{+/-}$ mouse embryo. *D*, high activity of the ERp57 promoter in the brain, lungs, and liver in an E18.5 an *ERp57*$^{+/-}$ mouse embryo. *E*, β-galactosidase staining of a wild-type E15.5 control embryo.

ERp57, was interrupted between introns 4 and 5 (nucleotides 14,083–14,084) with the pGT1.8TM cassette containing neomycin resistance and β-galactosidase genes (Fig. 1*A*). PCR analysis of genomic DNA using the specific sets of primers depicted in Fig. 1*A* allowed for determination of the genotypes of mice. Analysis of wild-type mice showed only a 797-base pair (bp) DNA product corresponding to the wild-type allele (Fig. 1*B*, primers *F2* and *R3*) and no DNA product with primers F1 and R3 (Fig. 1*B*). As expected, *ERp57*$^{-/-}$ mice showed a 1800-bp DNA product with primers F2 and

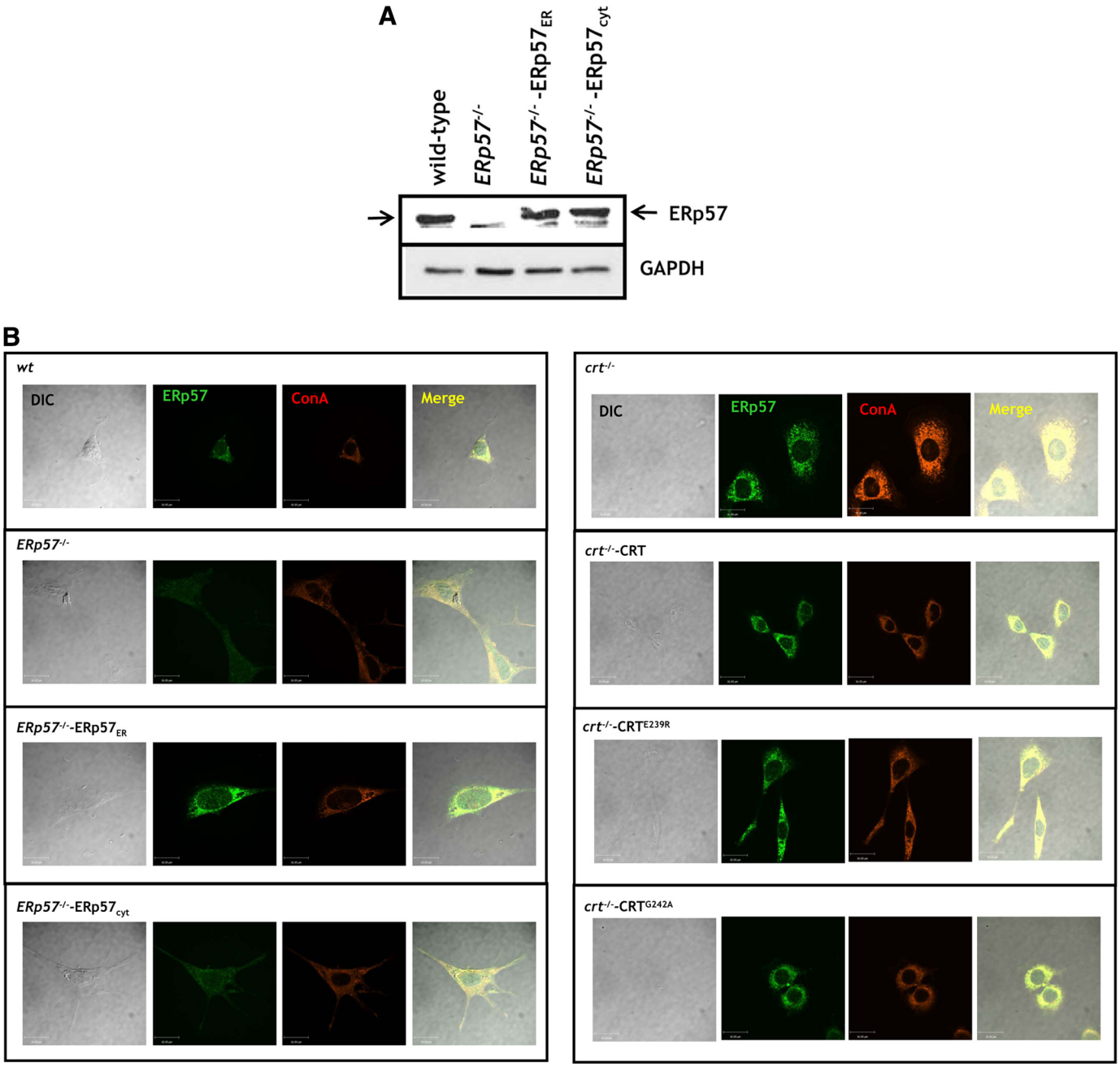

FIGURE 3. **Western blot and microscopy analysis of ERp57-deficient cells.** *A*, Western blot analysis of wild-type, ERp57-deficient cells ($ERp57^{-/-}$), and $ERp57^{-/-}$ cells expressing full-length recombinant ERp57 ($ERp57^{-/-}$-$ERp57_{ER}$) or cytoplasmic-targeted, no signal sequence ERp57 ($ERp57^{-/-}$-$ERp57_{cyt}$). Blots were probed with rabbit anti-ERp57 antibodies (*lower* protein band corresponds to a nonspecific immunoreactivity) and anti-GAPDH antibodies. In *B*, immunostaining of wild-type cells (*wt*), ERp57-deficient cells ($ERp57^{-/-}$), ERp57-deficient cells expressing full-length, ER-targeted recombinant ERp57 ($ERp57^{-/-}$-$ERp57_{ER}$), ERp57-deficient cells expressing cytoplasmically targeted recombinant ERp57 ($ERp57^{-/-}$-$ERp57_{cyt}$), calreticulin-deficient cells ($crt^{-/-}$), calreticulin-deficient cells expressing full-length calreticulin ($crt^{-/-}$-*CRT*), calreticulin-deficient cells expressing loss of ERp57 binding mutant ($crt^{-/-}$-CRT^{E239R}) or ERp57 binding mutant of calreticulin ($crt^{-/-}$-CRT^{G242A}). Cells were stained with anti-ERp57 antibodies and Texas Red-conjugated concanavalin A. In each panel images represent staining with anti-ERp57 antibodies, ConA staining, phase-contrast, and merged images of the cells. *Scale bar* = 16 μm. *C*, Western blot analysis of cell lysate, cytoplasmic, and microsomal (containing ER) fractions of wild-type, ERp57-deficient ($ERp57^{-/-}$), and ERp57-deficient cell lines expressing cytoplasmic targeted ERp57 ($ERp57^{-/-}$-$ERp57_{cyt}$). *D*, flow cytometry analysis of specific cell lines was carried out with anti-ERp57 antibodies. Wild-type, $ERp57^{-/-}$-$Erp57_{ER}$, $ERp57^{-/-}$-$Erp57_{CYS}$, $crt^{-/-}$, $crt^{-/-}$-*CRT*, $crt^{-/-}$-CRT^{E239R}, $crt^{-/-}$-CRT^{G242A} cell lines were used for the analysis. Results are presented as the relative mean florescence intensity after subtracting unspecific staining of $ERp57^{-/-}$ cells. *M2* represents the gate set on cells stained with antibody. *E*, electron microscopy analysis of wild-type and ERp57-deficient cells. The *arrows* indicate the location of the ER. *Scale bar* = 0.2 μm. *F*, Western blot analysis of ER chaperone proteins and oxidoreductases in wild-type (*wt*) and ERp57-deficient ($ERp57^{-/-}$) mouse embryonic fibroblasts. Antibodies used to probe the Western blot are indicated to the *right* of each panel. *Lower* protein band in the ERp57 lanes corresponds to a nonspecific immunoreactivity. *CNX*, calnexin; *CRT*, calreticulin.

R3 and no product with primers F1 and R3 (Fig. 1*B*). PCR-driven amplification of genomic DNA isolated from $ERp57^{+/-}$ mice produced both the 797- and 1,800-bp DNA products, indicating the presence of one copy of the wild-type allele and one copy of the targeted knock-out allele (Fig. 1*B*). Western blot analysis revealed that interruption of both

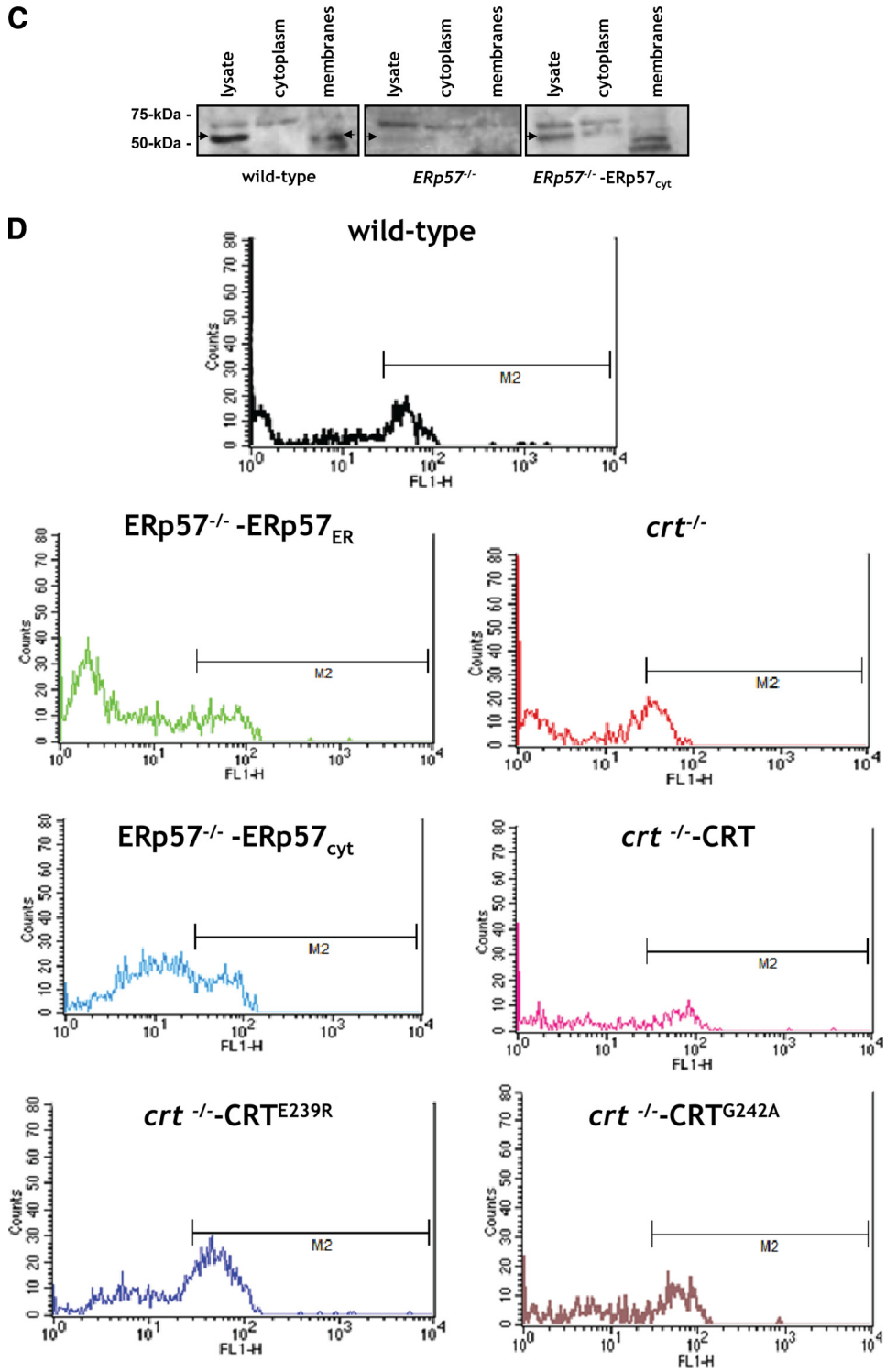

FIGURE 3—*continued*

alleles of the *ERp57* gene resulted in no detectable expression of ERp57 protein (Fig. 1*C*).

Chimeric mice were crossed with wild-type C57BL6 females to generate the first generation of heterozygotes. $ERp57^{+/-}$ B6/CD-1 mice were indistinguishable from wild-type animals. $ERp57^{+/-}$ males were intercrossed to $ERp57^{+/-}$ females to generate homozygote ($ERp57^{-/-}$) gene knock-out mice. We were unable to obtain any viable $ERp57^{-/-}$ pups from this cross. Viable embryos were obtained at E13.5 or earlier (Table 1). Analysis of embryos at or after E13.5 showed a deficiency in the number of $ERp57^{-/-}$ embryos indicating that a significant fraction of $ERp57^{-/-}$ embryos died earlier than E13.5. We concluded that the ERp57 gene knock-out was embryonic lethal and that ERp57 is essential for survival.

Developmental Activation of the ERp57 Gene—Histological analysis of E12.5 $ERp57^{-/-}$ embryos revealed that although there were no obvious gross morphological differences between $ERp57^{-/-}$ and wild-type embryos, the $ERp57^{-/-}$ embryos were markedly smaller than wild-type (Fig. 1*D*). To gain additional insight into the potential role of ERp57 during embryonic development, we carried out β-galactosidase reporter gene analysis. The transgenic animals used in this study were generated by insertion of a gene cassette containing the β-galactosidase reporter gene (Fig. 1*A*). To quantify transcriptional activation of the ERp57 gene we monitored expression of the β-galactosidase gene to evaluate ERp57 promoter activity in blastocysts and during embryonic development. Fig. 2*A* shows high expression and activity of β-galactosidase in blastocysts 3 days post-coitum indicating high expression of ERp57 during the early stages of blastocyst formation. High activation of the ERp57 gene was confined to the inner cell mass (Fig. 2*A*, *icm*) with relatively decreased activation of the gene in the blastocoel (Fig. 2*A*, *b*) and trophoblast (Fig. 2*A*, *t*). Next, $ERp57^{+/-}$ and wild-type embryos were harvested at different gestational stages and stained for β-galactosidase activity. Activation of the ERp57 gene, as reported by high activity of β-galactosidase, was observed as early as E13.5 (Fig. 2*B*). At E13.5 there was high activation in the lung and vertebra but a relatively low activity of the gene in the liver and heart (Fig. 2*B*). At E15.5 β-galactosidase reporter gene activity was the highest in the lungs with elevated activation also observed in the liver, vertebra, and intestine (Fig. 2*C*). However, the activity was strikingly absent in the heart, thymus, and neurological tissue including the brain (Fig. 2*C*). At later stages of embryonic

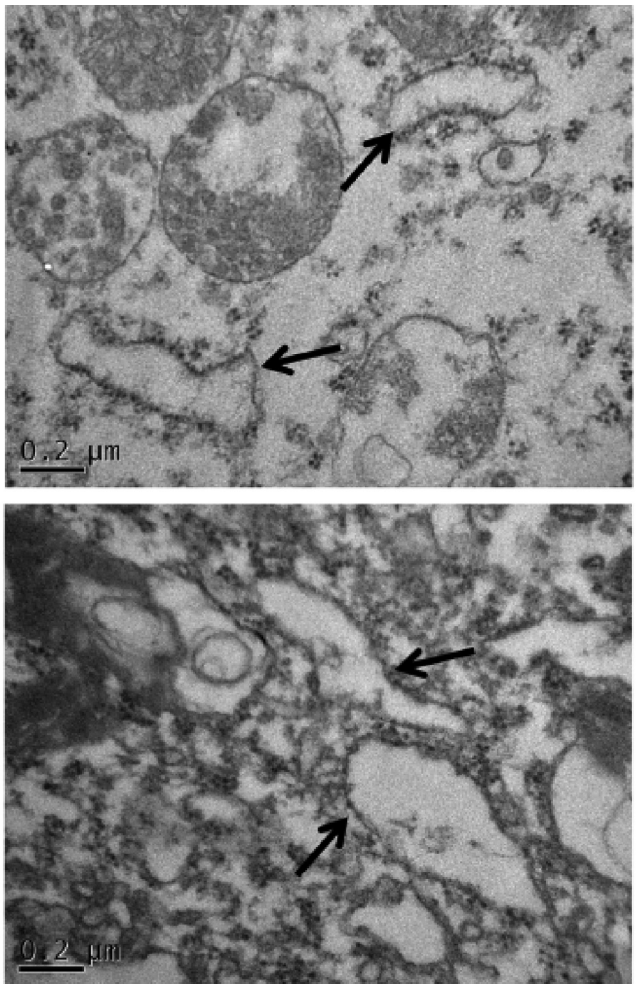

FIGURE 3—*continued*

development (E18.5), the pattern of activation of the ERp57 gene was significantly changed. Low activity of the ERp57 promoter was maintained in the heart, thymus, and skeletal muscle and high activity was observed in the lungs and liver (Fig. 2*D*). At E18.5 we now observed a significant increase in activation of the ERp57 gene in the brain, which was absent in the E13.5 (Fig. 2*D*). These data suggest that ERp57 may play a direct role during embryonic development, specifically in lung, liver, and vertebrae, and in the later developmental stages, in the brain.

The ER in ERp57-deficient Mouse Fibroblasts—To determine the effects of ERp57 deficiency on ER functions, we isolated mouse embryonic fibroblasts from ERp57-deficient and wild-type embryos. Some of the ERp57-deficient cells were transfected with expression vectors encoding full-length, ER-targeted ERp57, or cytoplasm-targeted ERp57 with no signal sequence and were designated *ERp57*$^{-/-}$-ERp57$_{ER}$ or *ERp57*$^{-/-}$-ERp57$_{cyt}$, respectively. As expected, Western blot analysis revealed that wild-type, *ERp57*$^{-/-}$-ERp57$_{ER}$, or *ERp57*$^{-/-}$-ERp57$_{cyt}$ cells contained immunoreactive ERp57 (Fig. 3*A*). Fig. 3*B* shows that wild-type and *ERp57*$^{-/-}$-57$_{ER}$ cells expressed ERp57 and that the protein was localized to an ER-like network. As expected, ERp57 was localized to the cytoplasmic compartment in ERp57-deficient cells expressing ERp57 without signal sequence (Fig. 3*B*, *ERp57*$^{-/-}$-ERp57$_{cyt}$). Cytoplasmic localization of ERp57 without signal sequence (ERp57$_{cyt}$) was further confirmed by biochemical fractionation of ERp57-deficient cells expressing ERp57 without signal sequence (*ERp57*$^{-/-}$-ERp57$_{cyt}$) (Fig. 3*C*). Finally, we carried out FACS analysis of different cells lines and showed that there was a small level of immunoreactive ERp57 detected on the cell surface of cell lines used in this study (Fig. 3*D*).

Morphologically, the ER appeared intact in all cell lines as judged by staining with Texas Red-conjugated concanavalin A or by electron microscopy analysis (Fig. 3, *B* and *E*). Western blot analysis demonstrated that there were no significant differences in the expression of ER chaperone proteins calreticulin, calnexin, Grp78/BiP, and Grp94 in the absence of ERp57 (Fig. 3*F*). Next we examined the impact of the absence of ERp57 on other oxidoreductase folding enzyme family members. Again there was no significant change in expression of PDI and or the PDI-like family of protein ERp19 in the absence of ERp57 (Fig. 3*F*). A slight increase in the level of ERp41 and decrease in the level of ERp54 was seen in the absence of ERp57 (Fig. 3*F*). Thus, the absence of ERp57 had no major impact on the expression of other ER chaperones or folding enzymes.

ER Ca^{2+} Homeostasis in the Absence of ERp57—The ER is the major Ca^{2+} store of the cell and calreticulin- or Grp94-deficient cells have impaired Ca^{2+} buffering and Ca^{2+} homeostasis (36–43). We examined, therefore, whether ERp57 deficiency had any effect on ER Ca^{2+} homeostasis. Wild-type, *ERp57*$^{-/-}$, and *ERp57*$^{-/-}$-ERp57$_{ER}$ mouse embryonic fibroblasts were stimulated with thapsigargin, an inhibitor of sarcoplasmic/endoplasmic reticulum Ca^{2+}-ATPase-type Ca^{2+} pumps or with bradykinin, a potent activator of the inositol 1,4,5-trisphosphate-dependent Ca^{2+} release channel located in the ER. When cells were stimulated with bradykinin, the peak amplitude and the duration of enhanced cytoplasmic Ca^{2+} concentration was comparable in wild-type, *ERp57*$^{-/-}$, and *ERp57*$^{-/-}$-ERp57$_{ER}$ cells (Fig. 4*A*). In *ERp57*$^{-/-}$ and *ERp57*$^{-/-}$-ERp57$_{ER}$ we observed a slight increase in Ca^{2+} concentration in response to thapsigargin when compared with wild-type (Fig. 4*B*), suggesting that there might be minor changes in ER Ca^{2+} capacity in the absence of ERp57. This might be due to an ERp57-dependent regulation of sarcoplasmic/endoplasmic reticulum Ca^{2+}-ATPase 2b activity (44).

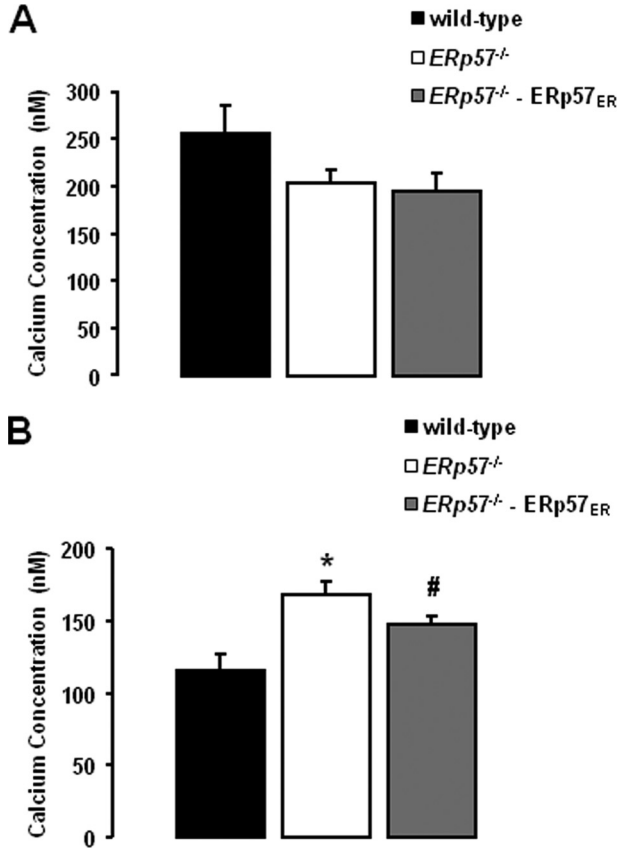

FIGURE 4. **Endoplasmic reticulum Ca^{2+} homeostasis in ERp57-deficient cells and cells expressing ER targeted ERp57.** Cytoplasmic Ca^{2+} concentration was measured in the wild-type and ERp57-deficient cells as described under "Experimental Procedures." *A*, Ca^{2+} released by bradykinin. In the absence of ERp57 (*white bar*) there was a decrease in bradykinin Ca^{2+} release but this not significantly different from wild-type (*black bar*). Bradykinin release is decreased in cells supplied with ER localized ERp57 ($ERp57^{-/-}$-$ERp57_{ER}$; *gray bar*) but this was not significantly different from wild-type cells. Data are presented as the mean ± S.D., $n = 4$. *B*, Ca^{2+} released by thapsigargin. In the absence of ERp57 ($ERp57^{-/-}$, *white bar*) and $ERp57^{-/-}$ cells transfected with expression vector encoding ERp57 ($ERp57^{-/-}$-$ERp57_{ER}$; *gray bar*), there was significantly more Ca^{2+} release. Data are presented as the mean ± S.D., $n = 4$. Two-sample, unpaired *t* test was performed. #, $p = 0.01$ *versus* wild-type and *, $p = 0.0065$ *versus* wild-type.

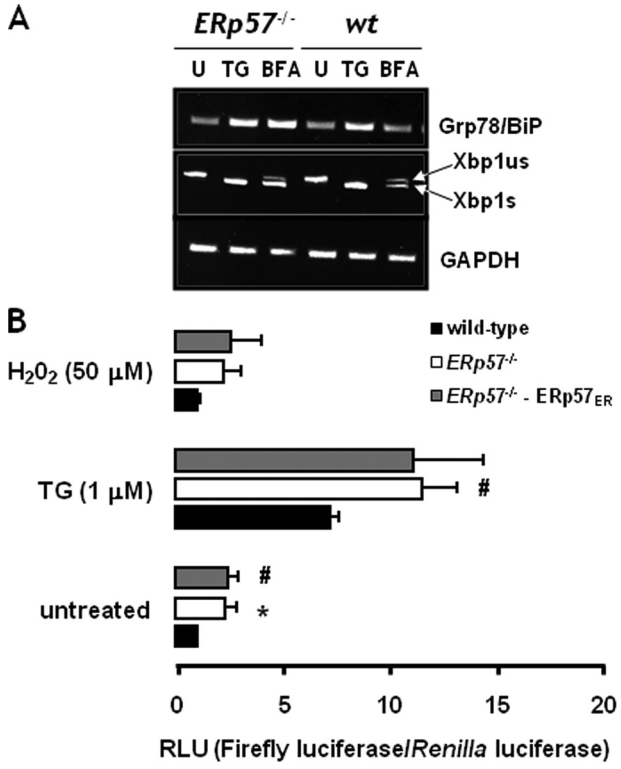

FIGURE 5. **Endoplasmic reticulum stress in the absence of ERp57.** ER stress was induced in wild-type and ERp57-deficient cells with thapsigargin (*TG;* 1 μM) or brefeldin A (*BFA;* 2.5 μM). *U* = untreated. *A*, RT-PCR analysis of Grp78/BiP mRNA and splicing of Xbp1 mRNA (2). Spliced (*Xbp1s*) and unspliced (*Xbp1 us*) forms of Xbp are indicated with *arrows*. RT-PCR of GAPDH mRNA was carried out to normalize for loading of agarose gels. *B*, quantitative analysis of splicing of the Xbp1 mRNA in wild-type and ERp57-deficient cells ($ERp57^{-/-}$). Cells were transfected with DNA plasmid reporting Xbp1 splicing. ER stress was induced with 1 μM thapsigargin (*TG*) or 50 μM H_2O_2. *Renilla* luciferase and firefly luciferase activities were measured and the relative ratio of firefly luciferase to *Renilla* luciferase activity in each cell lysate reported. Data are presented as the mean ± S.D., $n = 9$. *RLU*, relative light units. Two-sample, unpaired *t* test was performed. #, $p = 0.01$ *versus* wild-type and *, $p = 0.02$ *versus* wild-type.

The Unfolded Protein Response (UPR) in ERp57-deficient Cells—Next, we examined if the absence of ERp57 led to any induction of ER stress and consequently the initiation of the UPR. The UPR was examined by splicing analysis of mRNA encoding X-box-binding protein (Xbp1), which is cleaved and activated by ER stress-activated inositol-requiring enzyme-1 (2). As a control, ER stress was induced using a classical ER stress inducer, thapsigargin (2). In addition, we induced UPR/ER stress in wild-type and $ERp57^{-/-}$ cells with brefeldin A (BFA), an ER-Golgi trafficking inhibitor (45).

RT-PCR analysis was carried out to test for expression of Grp78/BiP mRNA and splicing of Xbp1, both markers of UPR. Non-stimulated wild-type and $ERp57^{-/-}$ cells did not have an increased level of Grp78/BiP mRNA nor was there any observable splicing of Xbp1 mRNA (Fig. 5*A*). As expected, thapsigargin induced complete splicing of Xbp1 (Fig. 5*A*, *Xbp1s*) as well as a significant increase in the level of Grp78/BiP mRNA (Fig. 5*A*). When wild-type and $ERp57^{-/-}$ cells were treated with BFA, there was incomplete splicing of Xbp1 with both unspliced (Fig. 5*A*, *Xbp1 us*) and spliced (Fig. 5*A*, *Xbp1s*) forms of Xbp1 mRNA detected. Interestingly, both the level of Grp78/BiP mRNA and the spliced form of Xbp1 were increased in $ERp57^{-/-}$ compared with wild-type cells (Fig. 5*A*), indicating that $ERp57^{-/-}$ cells were more sensitive to BFA-induced ER stress.

Next, we quantified Xbp1 splicing using a luciferase reporter system developed by Kaufman *et al.* (33). In this system, only the spliced form of the Xbp1 is in-frame with the luciferase reporter gene, therefore, high luciferase activity reports splicing of Xbp1 and increased ER stress (33). Fig. 5*B* shows that there was a small but significant increase in the UPR in $ERp57^{-/-}$ cells when compared with wild-type cells (Fig. 5*B*) and this was not rescued by expression of the recombinant ERp57 (Fig. 5*B*). Thapsigargin treatment significantly enhanced luciferase activity in wild-type, $ERp57^{-/-}$, and $ERp57^{-/-}$-$ERp57_{ER}$ cells (Fig. 5*B*). There was an 8-fold increase in UPR activation upon treatment with thapsigargin when compared with non-stimulated counterparts (Fig. 5*B*). Although there was a significant increase in ER stress in the absence of ERp57, this did not result in increased apoptosis in $ERp57^{-/-}$ cells (data not shown) indicating that ERp57-deficient cells experienced a tolerable level

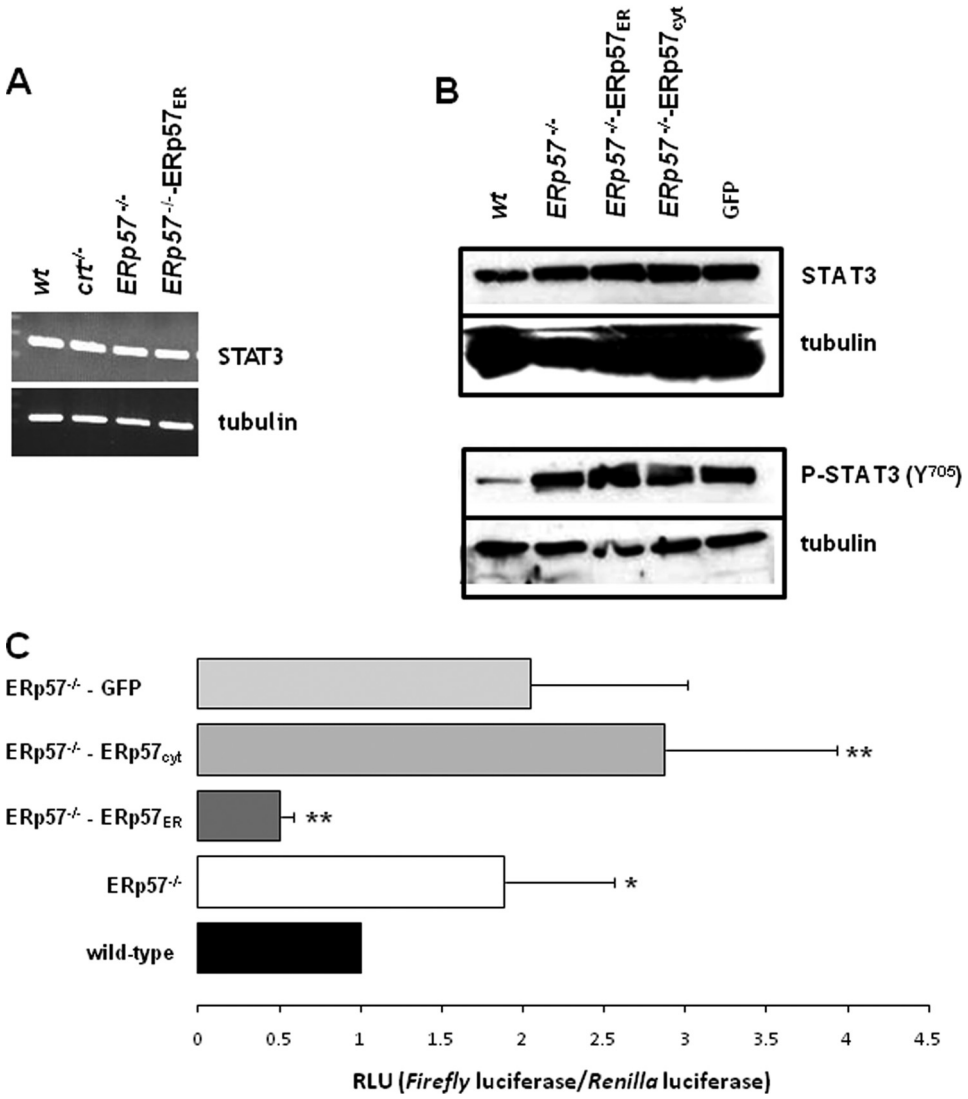

FIGURE 6. **STAT3 expression and activity in the absence of ERp57.** *A*, RT-PCR analysis of the STAT3 mRNA in wild-type (*wt*), calreticulin deletion ($crt^{-/-}$), $ERp57^{-/-}$-$ERp57_{ER}$, and $ERp57^{-/-}$-$ERp57_{cyt}$. *B*, Western blot analysis of STAT3 (*inactive*) and phosphorylated (Tyr^{705}) STAT3 (*active*) in wild-type (*wt*), $ERp57^{-/-}$-$ERp57_{ER}$, and $ERp57^{-/-}$-$ERp57_{cyt}$ cells. *C*, STAT3 activity in wild-type (*wt*), $ERp57^{-/-}$-$ERp57_{ER}$, and $ERp57^{-/-}$-$ERp57_{cyt}$ expressing cells. $ERp57^{-/-}$-GFP expressing cells were used a control. Cells were transfected with a plasmid containing the luciferase reporter gene under control of the STAT3-activated promoter. *Renilla* luciferase and firefly luciferase activities were measured as described under "Experimental Procedures," and the relative ratio of firefly luciferase to *Renilla* luciferase activity in each cell lysate presented. Data are the mean ± S.D. (wild-type, $n = 27$; $ERp57^{-/-}$, $n = 21$, $ERp57^{-/-}$-$ERp57_{ER}$, $n = 12$; $ERp57^{-/-}$-$ERp57_{cyt}$, $n = 12$; and $ERp57^{-/-}$-GFP, $n = 9$.) *RLU*, relative light units. Two-sample, unpaired *t* test was performed. *, $p = 0.0013$ *versus* wild-type and #, $p = 0.0001$ *versus* wild-type. **, $p = 0.0031$ *versus* $ERp57^{-/-}$-$ERp57_{ER}$.

of ER stress (46). ERp57 is one of the targets of oxidative stress induced by H_2O_2 (47), therefore, we also used H_2O_2 to induce ER stress in wild-type and $ERp57^{-/-}$ cells. H_2O_2 was not a very potent inducer of ER stress as there was only a slight increase in ER stress in cells treated with H_2O_2 (Fig. 5*C*). We concluded that ERp57 deficiency did not have a significant effect on ER morphology; expression of ER-associated chaperones and folding enzymes, ER stress, or apoptosis.

STAT3 Activation in the Absence of ERp57—Earlier reports indicate that ERp57, in addition to its function as an ER oxidoreductase folding enzyme, may play a role in modulation of the STAT3 signaling (6, 15, 48). It has been proposed that ERp57 forms complexes with both inactive and active STAT3, preventing STAT3 interaction with DNA and consequently leading to inhibition of the STAT3-dependent signaling pathway (6, 48). Therefore we took advantage of ERp57-deficient cells and examined whether the absence of ERp57 affected STAT3 signaling. STAT3 signaling was monitored using RT-PCR, Western blot analyses of inactive and active (phosphorylated-Tyr^{705}) STAT3, and luciferase activity assay for STAT3 activated promoter.

Fig. 6*A* shows that expression of STAT3 mRNA was not affected in the absence of ERp57 ($ERp57^{-/-}$) nor in ERp57-deficient cells transfected with ERp57 expression vector encoding ERp57 localized to the ER ($ERp57^{-/-}$-$ERp57_{ER}$). Tubulin expression was measured as a control. However, Western blot analysis showed increased levels of STAT3 protein and phospho-STAT3 (Tyr^{705}) (Fig. 6*B*). The level of phospho-STAT3 was not changed in $ERp57^{-/-}$-$ERp57_{ER}$ or $ERp57^{-/-}$-$ERp57_{cyt}$ (Fig. 6*B*). To quantify STAT3 activation we used plucTKS3 plasmid DNA containing the firefly luciferase reporter gene under the control of the STAT3 binding sites (34). Because ERp57 has been shown to inhibit STAT3 activity, we expected that STAT3-dependent activation of the promoter would result in high activity of luciferase in the absence of ERp57. Wild-type, $ERp57^{-/-}$, ERp57-deficient cells expressing ER-targeted ERp57 ($ERp57^{-/-}$-$ERp57_{ER}$), cytoplasmically targeted ERp57 (no N-terminal signal sequence, $ERp57^{-/-}$-$ERp57_{cyt}$), and green fluorescent protein (GFP) control were transfected with the luciferase reporter plasmid followed by analysis of luciferase activity. In non-stimulated $ERp57^{-/-}$ cells, there was a 2-fold increase in STAT3 activation (Fig. 6*C*) indicating that there was a link between ERp57 and STAT3 activity. Because STAT3 is a cytoplasmic/nuclear transcription factor found in the cytoplasm, for ERp57 to interact directly with STAT3 to form functional complexes, ERp57 would have to also be present in the cytoplasm. Therefore, we tested if the ER-targeted or cytoplasmically targeted ERp57 was effective in modulation of STAT3 signaling. High activity of STAT3 in $ERp57^{-/-}$ cells was partially rescued in ERp57-deficient cells expressing ER-targeted ERp57 (Fig. 6*C*, $ERp57^{-/-}$-$ERp57_{ER}$) but not in $ERp57^{-/-}$ cells expressing the cytoplasmi-

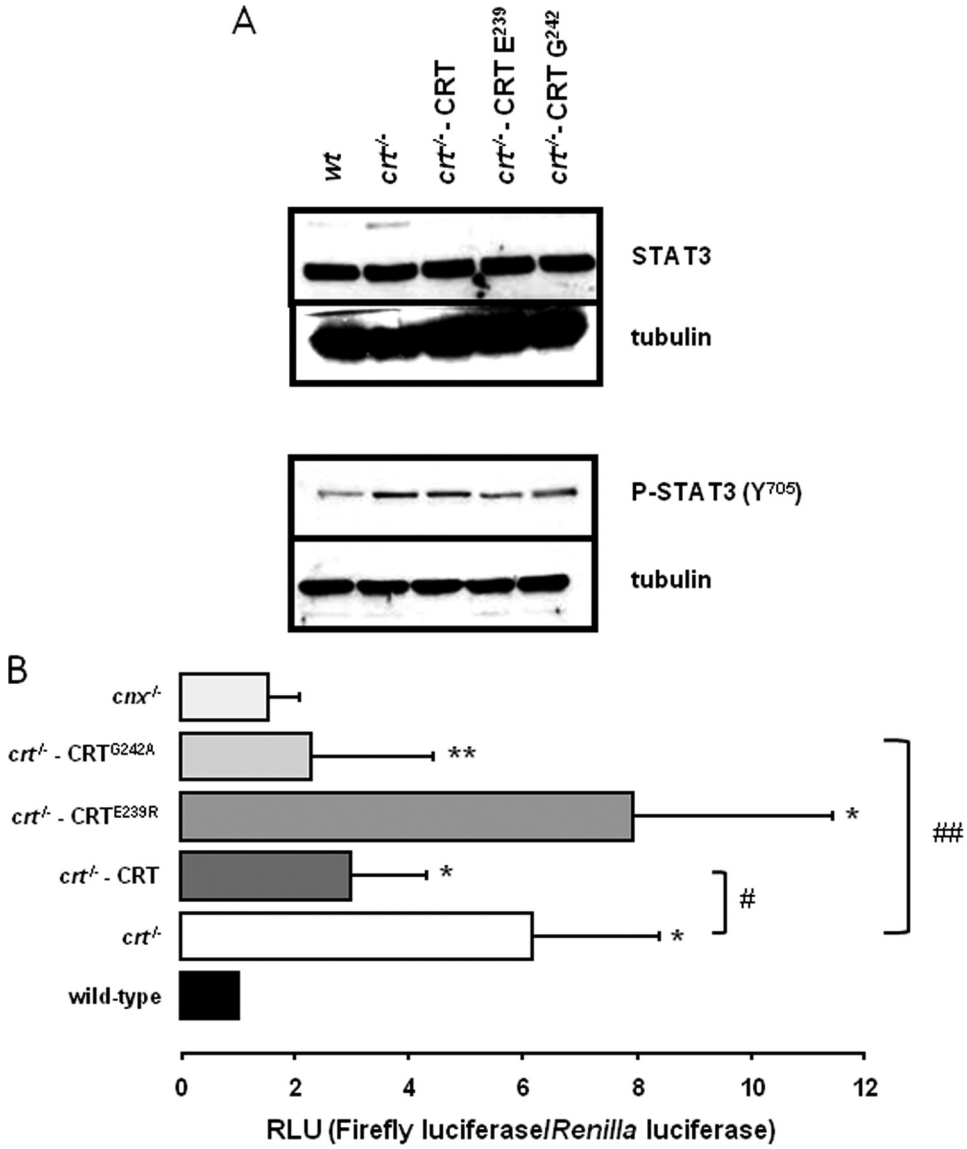

FIGURE 7. **Calreticulin enhances ERp57 effects on STAT3 activity.** *A*, Western blot analysis of STAT3 (*inactive*) and phosphorylated (Tyr^{705}) STAT3 (*active*) in wild-type (*wt*), calreticulin-deficient cells ($crt^{-/-}$), calreticulin-deficient cells with loss of ERp57 binding mutant ($crt^{-/-}$-CRT^{E239R}) or calreticulin-deficient cells with no loss of ERp57 binding ($crt^{-/-}$-CRT^{G242A}). Western blot analysis of tubulin was used as loading control. *B*, STAT3 activity in wild-type (*wt*), calreticulin-deficient cells ($crt^{-/-}$), calreticulin-deficient cells expression loss of ERp57 binding mutant ($crt^{-/-}$-CRT^{E239R}), or ERp57 no loss of binding mutant of calreticulin ($crt^{-/-}$-CRT^{G242A}). *Renilla* luciferase and firefly luciferase activities were measured as described under "Experimental Procedures" and the relative ratio of firefly luciferase to *Renilla* luciferase activity in each cell lysate presented. Data are the mean ± S.D. (wild-type, $n = 14$; $crt^{-/-}$, $n = 12$; $crt^{-/-}$-CRT, $n = 12$; $crt^{-/-}$-CRT^{G242A} $n = 4$; and $crt^{-/-}$-CRT^{E239R}, $n = 4$). *RLU*, relative light units. Two-sample, unpaired *t* test was performed. *, $p < 0.0001$ *versus* wild-type and **, $p = 0.02$ *versus* wild-type. #, $p = 0.0003$ *versus* $crt^{-/-}$. ##, $p = 0.0088$ *versus* $crt^{-/-}$.

Calreticulin Enhances ERp57 Modulation of STAT3 Signaling—ERp57 forms functional complexes with calreticulin to assist in folding and post-translational modification of newly synthesized proteins (3). We asked whether calreticulin may influence ERp57-dependent STAT3 activity. To do this we employed $crt^{-/-}$ cell lines expressing wild-type calreticulin or calreticulin mutants defective in binding ERp57 (32). In this study, we used a loss of ERp57 binding calreticulin-E239R mutant and a calreticulin-G242A mutant that has no loss in ERp57 binding (32). Western blot analysis showed that STAT3 or phospho-STAT3 (Tyr^{706}) expression was not affected by expression of calreticulin or calreticulin mutants in $crt^{-/-}$ cells (Fig. 7). Surprisingly, quantitative analysis of STAT3 activity using the luciferase reporter gene system showed high activity of STAT3 in $crt^{-/-}$ cells compared with wild-type counterparts (Fig. 7*B*), indicating that calreticulin may also affect STAT3 signaling. Fig. 7*B* shows that STAT3 was not affected in the absence of calnexin, a homologue of calreticulin. Expression of wild-type calreticulin (Fig. 7*B*, $crt^{-/-}$-*CRT*) or a calreticulin mutant interacting with ERp57 (Fig. 7*B*, $crt^{-/-}$-CRT^{G242A}) resulted in full recovery of STAT3 activity back to the level observed in wild-type cells (Fig. 7*B*, *wt*). In contrast, expression of the calreticulin mutant with a loss of ERp57 binding had no effect on STAT3 activity (Fig. 7*B*, $crt^{-/-}$-CRT^{E239R}), which remained high and at the same level as observed in calreticulin-deficient cells (Fig. 7*B*, $crt^{-/-}$). Taken together, these results indicate that ERp57-dependent modulation of STAT3 from the lumen of the ER requires calreticulin capable of forming complexes with ERp57.

cally targeted protein (Fig. 6*C*, $ERp57^{-/-}$-$ERp57_{cyt}$). As expected, expression of the recombinant GFP in ERp57-deficient cells did not have any effect on STAT3 transcriptional activity. Fig. 3*D* shows that there was a detectable level of immunoreactive ERp57 at the cell surface. However, we do not believe that this small fraction of ERp57 contributes to the modulation of STAT3 transcriptional activity because addition of purified ERp57 to cell cultures did not affect STAT3 transcriptional activity in the ERp57-deficient cells (supplemental Fig. S1). We concluded that ER-targeted ERp57 was the most effective in influencing STAT3 signaling, suggesting that ERp57 modulates STAT3 activity from the lumen of the ER.

DISCUSSION

In this study, we showed that deletion of the *Pdia3* gene, which encodes ERp57, was embryonic lethal at E13.5. Biochemical and cell biological analysis of ERp57-deficient cells indicated that the absence of ERp57 has no impact on ER morphology, expression of ER-associated chaperones and folding enzymes, ER stress, or apoptosis. However, we show that STAT3-dependent signaling was increased in the absence of ERp57 and

this could be rescued by expression of the ER-targeted ERp57, indicating that ERp57 affects STAT3 signaling from the lumen of the ER. This effect of ERp57 on the STAT3 pathway is further enhanced by an ER luminal complex formation between ERp57 and calreticulin. Increased STAT3 activity in the absence of ERp57 may contribute to embryonic lethality of *ERp57*$^{-/-}$ mice.

The ERp57 gene is differentially regulated during embryonic development indicating that the protein may play a direct role in development of specific tissues. This is in line with earlier observations of the expression of ER-associated ERp57 partner proteins, calreticulin and calnexin (2, 23). Calreticulin is predominately expressed in the heart during early stages of embryonic development and calreticulin-deficient mice die at E14.5 from impaired cardiac development (23). In contrast the calnexin gene is highly activated in neuronal tissue (2) and calnexin-deficient mice are born with neurological abnormalities (49). In this study, we showed that the ERp57 gene was highly active in the inner cell mass of blastocysts, an origin of fetus formation (50) and in the lung, liver, and brain during early stages of embryogenesis, suggesting that impaired development of these tissues may, at least in part, contribute to *ERp57*$^{-/-}$ embryonic lethality. The high expression of ERp57 in the lungs seen in this study is of interest because it has recently been reported that ERp57 is decreased in a neonatal rat model of hyperoxia-induced lung injury and cultured cells (47). Small interfering RNA knockdown of ERp57 in human endothelial cells resulted in cellular protection against hyperoxia and tunicamycin-induced caspase-3 activation apoptosis, suggesting that ERp57 has a role in the regulation of apoptosis (47).

Garbi *et al.* (4) carried out a targeted deletion of the ERp57 gene in mouse B cells. They also reported no *ERp57*$^{-/-}$ offspring, indicating that ERp57 deficiency might be embryonic lethal. Here we investigated embryonic development in the absence of ERp57 and showed that *ERp57*$^{-/-}$ was embryonic lethal at E13.5. Interestingly, deletion of ERp57 in B cells in mice results in normal B cell development, proliferation, and antibody production indicating that ERp57 is not required for glycoprotein folding in B cells (4). However, there is aberrant assembly of the peptide loading complex, showing that ERp57 is involved in the assembly of the peptide loading complex and contributes both qualitatively and quantitatively to MHC class I antigen presentation *in vivo*. This supports earlier observations that ERp57 is critically involved in the early folding events of MHC class I heavy chain (5, 14). The role of ERp57 in MHC class I biogenesis and assembly is further supported by ERp57 small interfering RNA studies (5, 51, 52).

In addition to its role as a folding enzyme in quality control in the secretory pathway, ERp57 is reported to affect STAT3 signaling (12). This may be due to formation of inhibitory complexes between the ERp57 and STAT3 protein either in the cytoplasm or nucleus (6, 15, 48, 53, 54). Furthermore, in avian and mammalian cells, DNA-protein cross-linking experiments indicate that ERp57 is nuclear and interacts directly with DNA (15). *In vitro* experiments in HeLa cells showed that ERp57 preferentially binds DNA sequences having characteristic scaffold/matrix-associated regions (55). Finally, the protein has also been suggested to be present on the cell surface and in the cytoplasm (6, 14–17). Using FACS analysis we detected some immunoreactive ERp57 on the surface of cells used in this study. However, it is unlikely that cell surface ERp57 affects STAT3 transcriptional activity as addition of extracellular ERp57 did not affect STAT3 function (supplemental Fig. S1). The conundrum then is: how does ERp57 gain access to the cytoplasm/nucleus to influence STAT3 activity when its N-terminal signal sequence should direct it to the ER and its C-terminal QDEL ER retrieval motif should keep it there? To address this question, we took advantage of available ERp57-deficient cells and tested, for the first time, STAT3 signaling in the absence of ERp57. Analysis of STAT3-dependent expression of the luciferase reporter gene in ERp57-deficient cells revealed that ERp57 indeed affects STAT3 signaling. Most importantly, we showed that the ER but not the cytoplasmic form of ERp57 was effective in inhibition of STAT3 activity. This effect is specific to ERp57, because transfection of ER-targeted GFP or calnexin did not have any effect on the STAT3 activity.

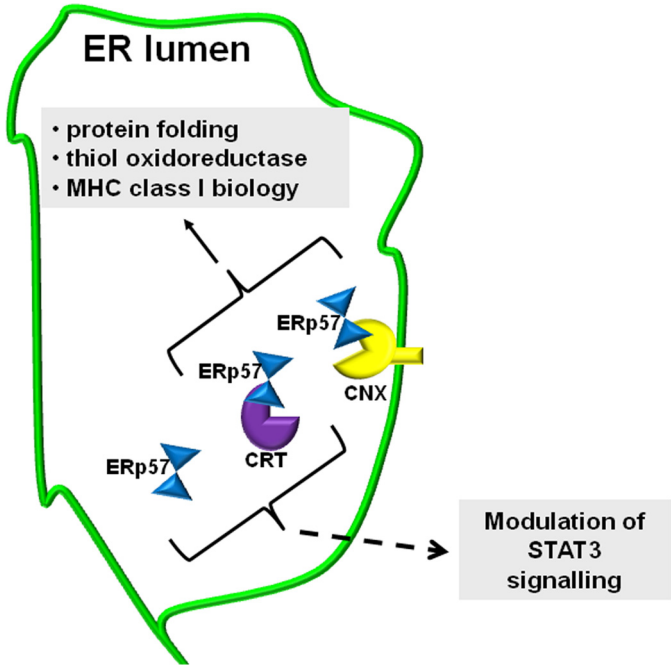

FIGURE 8. **A model of the relationship between STAT3, ERp57, and calreticulin.** This model shows cross-talk between ERp57, calreticulin, and STAT3 signaling. ERp57 forms functional complexes with calnexin and calreticulin to promote protein folding, disulfide bond formation, and isomerization. ERp57 is also critical for MHC class I biosynthesis and assembly. A model shows that ERp57, from the lumen of the ER, also affects STAT3 signaling and functions as a STAT3 inhibitor. ERp57-dependent modulation of STAT3 is enhanced by complex formation between ERp57 and calreticulin.

Fig. 8 shows a model of ERp57 function in the lumen of the ER. ERp57 is an ER resident folding enzyme involved in oxidative folding of glycoproteins in the ER, biosynthesis of the MHC class I, and as a component of the loading complex (14). In this study, we showed that ERp57 also affects STAT3 signaling from the lumen of the ER (Fig. 8). It is not clear at present how ERp57 affected STAT3 signaling, but our work indicates that the inhibitory function of ERp57 was significantly enhanced by interaction with another ER resident luminal protein, calreticulin (Fig. 8). The two proteins form functional complexes involved in folding and post-translational modification of

newly synthesized (glyco)proteins (42). Our results indicate that ERp57-dependent modulation of STAT3 activity also depends on the formation of ERp57-calreticulin complexes in the lumen of the ER. Interestingly, ERp57-calreticulin complex formation might also be important for cell surface targeting of these ER proteins (56).

The molecular mechanisms of ERp57-dependent signaling from the ER are not presently clear, however, several other cellular processes are controlled by "ER signaling." For example, cholesterol homeostasis is controlled by ER-nuclear signaling via sterol-regulated proteolysis of ER membrane-bound transcription factors called sterol regulatory element-binding proteins (57). The UPR is also regulated by ER-associated kinases, which transduce their signals from the ER to affect gene expression in the nucleus (58). One critical aspect of Ca^{2+} homeostasis is involved in store-operated Ca^{2+} influx resulting from ER-dependent activation of the plasma membrane Ca^{2+} channel (59). Transcriptional activity of steroid receptors is also modulated by ER luminal proteins (60). Here we report, for the first time, that the STAT3-dependent pathway may also be modulated by signaling from the ER.

Acknowledgments—The superb technical assistance of Monika Dabrowska and Alison Thorne is greatly appreciated. We thank R. Kaufman and J. Jung for plasmid DNA.

REFERENCES

1. Bedard, K., Szabo, E., Michalak, M., and Opas, M. (2005) *Int. Rev. Cytol.* **245,** 91–121
2. Coe, H., Bedard, K., Groenendyk, J., Jung, J., and Michalak, M. (2008) *Cell Stress Chaperones* **13,** 497–507
3. Hebert, D. N., and Molinari, M. (2007) *Physiol. Rev.* **87,** 1377–1408
4. Garbi, N., Tanaka, S., Momburg, F., and Hammerling, G. J. (2006) *Nat. Immun.* **7,** 93–102
5. Zhang, Y., Baig, E., and Williams, D. B. (2006) *J. Biol. Chem.* **281,** 14622–14631
6. Guo, G. G., Patel, K., Kumar, V., Shah, M., Fried, V. A., Etlinger, J. D., and Sehgal, P. B. (2002) *J. Interferon Cytokine Res.* **22,** 555–563
7. Hetz, C., Russelakis-Carneiro, M., Wälchli, S., Carboni, S., Vial-Knecht, E., Maundrell, K., Castilla, J., and Soto, C. (2005) *J. Neurosci.* **25,** 2793–2802
8. Hirano, N., Shibasaki, F., Sakai, R., Tanaka, T., Nishida, J., Yazaki, Y., Takenawa, T., and Hirai, H. (1995) *Eur. J. Biochem.* **234,** 336–342
9. Khanal, R. C., and Nemere, I. (2007) *Curr. Med. Chem.* **14,** 1087–1093
10. Mazzarella, R. A., Marcus, N., Haugejorden, S. M., Balcarek, J. M., Baldassare, J. J., Roy, B., Li, L. J., Lee, A. S., and Green, M. (1994) *Arch. Biochem. Biophys.* **308,** 454–460
11. Muhlenkamp, C. R., and Gill, S. S. (1998) *Toxicol. Appl. Pharmacol.* **148,** 101–108
12. Ndubuisi, M. I., Guo, G. G., Fried, V. A., Etlinger, J. D., and Sehgal, P. B. (1999) *J. Biol. Chem.* **274,** 25499–25509
13. Wyse, B., Ali, N., and Ellison, D. H. (2002) *Am. J. Physiol. Renal Physiol.* **282,** F424–F430
14. Wearsch, P. A., and Cresswell, P. (2008) *Curr. Opin. Cell Biol.* **20,** 624–631
15. Coppari, S., Altieri, F., Ferraro, A., Chichiarelli, S., Eufemi, M., and Turano, C. (2002) *J. Cell. Biochem.* **85,** 325–333
16. Grillo, C., Coppari, S., Turano, C., and Altieri, F. (2002) *Biochem. Biophys. Res. Commun.* **295,** 67–73
17. Altieri, F., Maras, B., Eufemi, M., Ferraro, A., and Turano, C. (1993) *Biochem. Biophys. Res. Commun.* **194,** 992–1000
18. Boengler, K., Hilfiker-Kleiner, D., Drexler, H., Heusch, G., and Schulz, R. (2008) *Pharmacol. Ther.* **120,** 172–185
19. Lim, C. P., and Cao, X. (2006) *Mol. Biosyst.* **2,** 536–550
20. Fischer, P., and Hilfiker-Kleiner, D. (2007) *Basic Res. Cardiol.* **102,** 393–411
21. Nichols, J., Evans, E. P., and Smith, A. G. (1990) *Development* **110,** 1341–1348
22. Mery, L., Mesaeli, N., Michalak, M., Opas, M., Lew, D. P., and Krause, K. H. (1996) *J. Biol. Chem.* **271,** 9332–9339
23. Mesaeli, N., Nakamura, K., Zvaritch, E., Dickie, P., Dziak, E., Krause, K. H., Opas, M., MacLennan, D. H., and Michalak, M. (1999) *J. Cell Biol.* **144,** 857–868
24. Reddy, R. K., Dubeau, L., Kleiner, H., Parr, T., Nichols, P., Ko, B., Dong, D., Ko, H., Mao, C., DiGiovanni, J., and Lee, A. S. (2002) *Cancer Res.* **62,** 7207–7212
25. Suter, D. M., Cartier, L., Bettiol, E., Tirefort, D., Jaconi, M. E., Dubois-Dauphin, M., and Krause, K. H. (2006) *Stem Cells* **24,** 615–623
26. Milner, R. E., Baksh, S., Shemanko, C., Carpenter, M. R., Smillie, L., Vance, J. E., Opas, M., and Michalak, M. (1991) *J. Biol. Chem.* **266,** 7155–7165
27. Milner, R. E., Michalak, M., and Wang, L. C. (1991) *Biochim. Biophys. Acta* **1063,** 120–128
28. Nakamura, K., Bossy-Wetzel, E., Burns, K., Fadel, M. P., Lozyk, M., Goping, I. S., Opas, M., Bleackley, R. C., Green, D. R., and Michalak, M. (2000) *J. Cell Biol.* **150,** 731–740
29. Knoblach, B., Keller, B. O., Groenendyk, J., Aldred, S., Zheng, J., Lemire, B. D., Li, L., and Michalak, M. (2003) *Mol. Cell. Proteomics* **2,** 1104–1119
30. Okiyoneda, T., Harada, K., Takeya, M., Yamahira, K., Wada, I., Shuto, T., Suico, M. A., Hashimoto, Y., and Kai, H. (2004) *Mol. Biol. Cell* **15,** 563–574
31. Lozyk, M. D., Papp, S., Zhang, X., Nakamura, K., Michalak, M., and Opas, M. (2006) *BMC Dev. Biol.* **6,** 54
32. Martin, V., Groenendyk, J., Steiner, S. S., Guo, L., Dabrowska, M., Parker, J. M., Müller-Esterl, W., Opas, M., and Michalak, M. (2006) *J. Biol. Chem.* **281,** 2338–2346
33. Back, S. H., Lee, K., Vink, E., and Kaufman, R. J. (2006) *J. Biol. Chem.* **281,** 18691–18706
34. Chung, Y. H., Cho, N. H., Garcia, M. I., Lee, S. H., Feng, P., and Jung, J. U. (2004) *J. Virol.* **78,** 6489–6497
35. Turkson, J., Bowman, T., Garcia, R., Caldenhoven, E., De Groot, R. P., and Jove, R. (1998) *Mol. Cell. Biol.* **18,** 2545–2552
36. Nakamura, K., Zuppini, A., Arnaudeau, S., Lynch, J., Ahsan, I., Krause, R., Papp, S., De Smedt, H., Parys, J. B., Muller-Esterl, W., Lew, D. P., Krause, K. H., Demaurex, N., Opas, M., and Michalak, M. (2001) *J. Cell Biol.* **154,** 961–972
37. Lièvremont, J. P., Rizzuto, R., Hendershot, L., and Meldolesi, J. (1997) *J. Biol. Chem.* **272,** 30873–33089
38. Argon, Y., and Simen, B. B. (1999) *Semin. Cell Dev. Biol.* **10,** 495–505
39. Lebeche, D., Lucero, H. A., and Kaminer, B. (1994) *Biochem. Biophys. Res. Commun.* **202,** 556–561
40. Lucero, H. A., and Kaminer, B. (1999) *J. Biol. Chem.* **274,** 3243–3251
41. Lucero, H. A., Lebeche, D., and Kaminer, B. (1998) *J. Biol. Chem.* **273,** 9857–9863
42. Michalak, M., Groenendyk, J., Szabo, E., Gold, L. I., and Opas, M. (2009) *Biochem. J.* **417,** 651–666
43. Reddy, R. K., Lu, J., and Lee, A. S. (1999) *J. Biol. Chem.* **274,** 28476–28483
44. Li, Y., and Camacho, P. (2004) *J. Cell Biol.* **164,** 35–46
45. Alvarez, C., and Sztul, E. S. (1999) *Eur. J. Cell Biol.* **78,** 1–14
46. Rutkowski, D. T., Arnold, S. M., Miller, C. N., Wu, J., Li, J., Gunnison, K. M., Mori, K., Sadighi Akha, A. A., Raden, D., and Kaufman, R. J. (2006) *PLoS Biol.* **4,** e374
47. Xu, D., Perez, R. E., Rezaiekhaligh, M. H., Bourdi, M., and Truog, W. E. (2009) *Am. J. Physiol. Lung Cell. Mol. Physiol.* **297,** L44–L51
48. Eufemi, M., Coppari, S., Altieri, F., Grillo, C., Ferraro, A., and Turano, C. (2004) *Biochem. Biophys. Res. Commun.* **323,** 1306–1312
49. Denzel, A., Molinari, M., Trigueros, C., Martin, J. E., Velmurgan, S., Brown, S., Stamp, G., and Owen, M. J. (2002) *Mol. Cell. Biol.* **22,** 7398–7404
50. Ghassemifar, M. R., Eckert, J. J., Houghton, F. D., Picton, H. M., Leese, H. J., and Fleming, T. P. (2003) *Mol. Hum. Reprod.* **9,** 245–252
51. Garbi, N., Hämmerling, G., and Tanaka, S. (2007) *Curr. Opin. Immunol.*

19, 99–105
52. Zhang, Y., Kozlov, G., Pocanschi, C. L., Brockmeier, U., Ireland, B. S., Maattanen, P., Howe, C., Elliott, T., Gehring, K., and Williams, D. B. (2009) *J. Biol. Chem.* **284,** 10160–10173
53. Sehgal, P. B., Guo, G. G., Shah, M., Kumar, V., and Patel, K. (2002) *J. Biol. Chem.* **277,** 12067–12074
54. Kita, K., Okumura, N., Takao, T., Watanabe, M., Matsubara, T., Nishimura, O., and Nagai, K. (2006) *FEBS Lett.* **580,** 199–205
55. Ferraro, A., Altieri, F., Coppari, S., Eufemi, M., Chichiarelli, S., and Turano, C. (1999) *J. Cell. Biochem.* **72,** 528–539
56. Panaretakis, T., Joza, N., Modjtahedi, N., Tesniere, A., Vitale, I., Durchschlag, M., Fimia, G. M., Kepp, O., Piacentini, M., Froehlich, K. U., van Endert, P., Zitvogel, L., Madeo, F., and Kroemer, G. (2008) *Cell Death Differ.* **15,** 1499–1509
57. Horton, J. D., Goldstein, J. L., and Brown, M. S. (2002) *J. Clin. Invest.* **109,** 1125–1131
58. Schröder, M., and Kaufman, R. J. (2005) *Annu. Rev. Biochem.* **74,** 739–789
59. Putney, J. W., Jr. (2007) *Cell Calcium* **42,** 103–110
60. Burns, K., Duggan, B., Atkinson, E. A., Famulski, K. S., Nemer, M., Bleackley, R. C., and Michalak, M. (1994) *Nature* **367,** 476–480